Journal of Physics: Conference Series

PAPER • OPEN ACCESS

Vibration Prediction Method of Electric Machines by using Experimental Transfer Function and Magnetostatic Finite Element Analysis

To cite this article: A Saito *et al* 2016 *J. Phys.: Conf. Ser.* **744** 012088

View the article online for updates and enhancements.

You may also like

- Method for extracting the free vibration response of transmission tower
Long Zhao, Guanru Wen, Zhicheng Liu et al.
- Electroelastic modeling and experimental validations of piezoelectric energy harvesting from broadband random vibrations of cantilevered bimorphs
S Zhao and A Erturk
- Impact vibration properties of locally resonant fluid-conveying pipes
Bing Hu, , Fu-Lei Zhu et al.

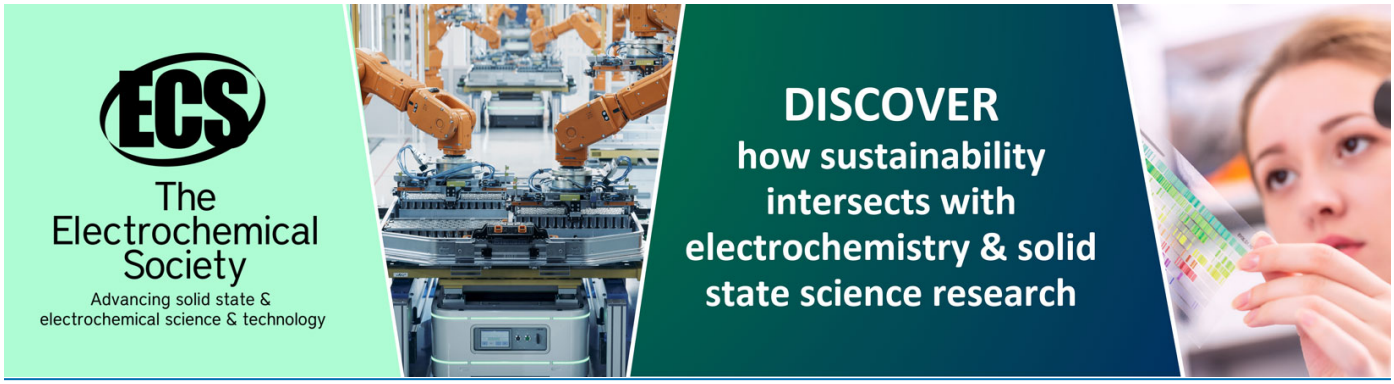

This content was downloaded from IP address 3.144.48.135 on 03/05/2024 at 04:47

Vibration Prediction Method of Electric Machines by using Experimental Transfer Function and Magnetostatic Finite Element Analysis

A Saito, M Kuroishi and H Nakai

Toyota Central R&D Labs., Inc., 41-1 Yokomichi, Nagakute, Aichi 480-1192, Japan

E-mail: akira-saito@mosk.tytlabs.co.jp

Abstract. This paper concerns the noise and structural vibration caused by rotating electric machines. Special attention is given to the magnetic-force induced vibration response of interior-permanent magnet machines. In general, to accurately predict and control the vibration response caused by the electric machines, it is inevitable to model not only the magnetic force induced by the fluctuation of magnetic fields, but also the structural dynamic characteristics of the electric machines and surrounding structural components. However, due to complicated boundary conditions and material properties of the components, such as laminated magnetic cores and varnished windings, it has been a challenge to compute accurate vibration response caused by the electric machines even after their physical models are available. In this paper, we propose a highly-accurate vibration prediction method that couples experimentally-obtained discrete structural transfer functions and numerically-obtained distributed magnetic-forces. The proposed vibration synthesis methodology has been applied to predict vibration responses of an interior permanent magnet machine. The results show that the predicted vibration response of the electric machine agrees very well with the measured vibration response for several load conditions, for wide frequency ranges.

1. Introduction

In recent years, suppression of undesirable noise and vibration caused by electric machines has been an important research issue in auto industry. It is due to the increasing ubiquity of electrified components inside a passenger vehicle. For instance, hybrid electric vehicles use the electric machines in conjunction with internal combustion engines for propulsion of the vehicles. Pure electric vehicles use the electric machines as the sole driving source of the vehicles. Other in-vehicle components, such as air conditioning systems and power steering systems are also gradually being replaced by the electrified counterparts. Therefore, engineers need to deal with classic yet challenging task of reducing noise and vibrations caused by the electric machines.

Modern vibration prediction methods for the electric machines are based on finite element (FE) frameworks. Namely, FEAs for magnetic fields and elastic displacement fields are conducted, where the two physical domains are either strongly or weakly coupled to each other. The strong coupling approach takes into account the effect of the magnetic field on the elastic field as well as the effect of the elastic field on the magnetic field [1]. This class of methods is required when we need to analyze phenomena such as stress-dependent nonlinearity of magnetic cores, or the displacement is so large that the change in the geometry affects the magnetic field. Due mostly to the computational cost of such approaches, however, many of the vibration analysis methods for the electric machines employ the weak coupling approach [2–4]. Namely, we first conduct the magnetic FEA to obtain magnetic forces. The structural

Content from this work may be used under the terms of the Creative Commons Attribution 3.0 licence. Any further distribution of this work must maintain attribution to the author(s) and the title of the work, journal citation and DOI.
Published under licence by IOP Publishing Ltd

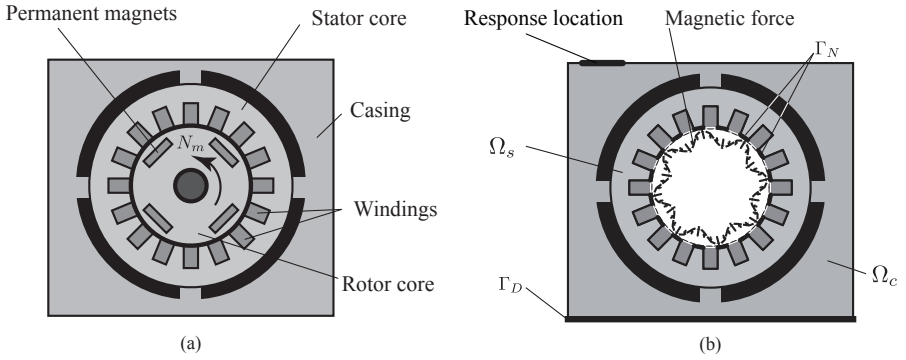

Figure 1. Schematics of the electric machine: (a) typical configuration of the IPM machines, (b) definition of the computational domain.

dynamic FEA is then conducted to compute vibration response due to the magnetic forces. These analysis methods based on FEAs are, however, prone to various types of errors such as modeling and discretization errors. Most importantly, the use of laminated electrical steel sheets [5–9] and windings [10] complicates the modeling of the structural dynamic characteristics of the electric machines. Therefore, replacement of the structural dynamic model with experimentally obtained quantities has been proposed by several researchers [11–14]. Such methodology is useful for analyzing the vibration response of *existing products*, instead of predicting it at the design-phase of the products. The power of such methodologies comes into play when one needs to optimize control schemes or rotor structure yet vibration response of the motor stator/housing also needs to be evaluated with high fidelity. Since conducting accurate vibration analysis of the motor stator/housing is difficult as mentioned above, such consideration is not possible in reality. The method proposed in this paper enables ones to conduct such analysis, which is based on: weak coupling approach between magnetic and displacement fields; and representation of structural dynamic characteristics using experimentally obtained transfer functions. The novelty of the proposed methodology is that the structural dynamic model can be coupled directly with the magnetostatic FEAs by utilizing the magnetic forces. This paper is organized as follows. In Section 2, mathematical background of the proposed method is described. In Section 3, a detailed procedure of the proposed method is provided. The result of experimental validation is given in Section 4. Conclusions of the paper are given in Section 5.

2. Mathematical formulation

In this paper, we use an interior permanent magnet machine (IPM) as an example of the electric machines (Fig. 1(a)). Denoting the domains occupied by the motor stator and the casing as $\Omega_s \subset \mathbb{R}^3$ and $\Omega_c \subset \mathbb{R}^3$ respectively, the assembly of the motor core and the casing is represented as $\Omega = \Omega_s \cup \Omega_c$ (Fig. 1(b)). Now consider the forced vibration problem of the assembly that is subject to magnetic-force excitation on the surface of the stator's teeth. We assume that the vibration is so small that the strain induced by the displacement is linear, and any effect caused by the deformation of the core on the magnetic field can be ignored. Denoting the displacement field of the assembly as $\boldsymbol{u}(\boldsymbol{x}, t)$ where $\boldsymbol{x} \in \mathbb{R}^3$, the governing equation of motion of the displacement field can be written in strong form as follows:

$$\rho\ddot{\boldsymbol{u}}(\boldsymbol{x}, t) + \alpha\rho\dot{\boldsymbol{u}}(\boldsymbol{x}, t) = \boldsymbol{\nabla} \cdot \boldsymbol{\tau}(\boldsymbol{u}, \dot{\boldsymbol{u}}) \text{ in } \Omega, \tag{1}$$

$$\boldsymbol{u}(\boldsymbol{x}, t) = \boldsymbol{0} \text{ on } \Gamma_D, \tag{2}$$

$$\boldsymbol{\sigma} \cdot \boldsymbol{n}(\boldsymbol{x}) = \boldsymbol{f}(\boldsymbol{x}, t) \text{ on } \Gamma_N, \tag{3}$$

where Γ_D denotes the Dirichlet boundary where the fixed-boundary condition is applied, Γ_N denotes the Neumann boundary where the magnetic force is applied, ρ is the density, $\boldsymbol{f}(\boldsymbol{x}, t)$ is the vector of magnetic

force density, $\boldsymbol{n}$ is the normal vector pointing outward the surface of the stator teeth, $\boldsymbol{\tau}$ is a stress tensor defined as

$$\boldsymbol{\tau}(\boldsymbol{u}, \dot{\boldsymbol{u}}) = \boldsymbol{\sigma}(\boldsymbol{u}) + \beta\boldsymbol{\sigma}(\dot{\boldsymbol{u}}). \tag{4}$$

α and β are the damping coefficients of the Rayleigh-damping model. $\boldsymbol{\sigma}(\boldsymbol{u})$ is the Cauchy stress tensor determined based on the constitutive relationship:

$$\boldsymbol{\sigma}(\boldsymbol{u}) = \boldsymbol{C} : \boldsymbol{\varepsilon}(\boldsymbol{u}), \tag{5}$$

where $\boldsymbol{C}$ is the elasticity tensor, ":" denotes a double dot product, and the strain tensor $\boldsymbol{\varepsilon}$ is defined as:

$$\boldsymbol{\varepsilon}(\boldsymbol{u}) = \frac{1}{2}\left(\boldsymbol{\nabla u} + (\boldsymbol{\nabla u})^{\mathrm{T}}\right). \tag{6}$$

With the quasi-static assumption, the magnetic force density is computed by solving the following two-dimensional magnetostatic problem:

$$\boldsymbol{\nabla} \times \boldsymbol{H}(\boldsymbol{x}, t) = \boldsymbol{J}(\boldsymbol{x}, t), \tag{7}$$

$$\boldsymbol{B}(\boldsymbol{x}, t) = \boldsymbol{\nabla} \times \boldsymbol{A}(\boldsymbol{x}, t), \tag{8}$$

$$\boldsymbol{B} = \boldsymbol{B}(\boldsymbol{H}), \tag{9}$$

where $\boldsymbol{H}$ is the magnetic field, $\boldsymbol{J}$ is the vector of current density, $\boldsymbol{A}$ is the magnetic vector potential, and $\boldsymbol{B}$ is the magnetic flux density. In this paper, it is assumed that $\boldsymbol{J}$ and $\boldsymbol{A}$ only have components that are parallel to the axial direction of the electric machine. Namely, denoting the axial direction as z, and the unit vector along z as $\boldsymbol{k}$, $\boldsymbol{J} = J_z\boldsymbol{k}$ and $\boldsymbol{A} = A_z\boldsymbol{k}$. Equation (9) is a material-dependent nonlinear constitutive relationship between $\boldsymbol{B}$ and $\boldsymbol{H}$. The quantity that couples the displacement field and the magnetic field is the vector of magnetic force density $\boldsymbol{f}(\boldsymbol{x}, t)$ in Eq. (3), which is determined from the Maxwell's stress tensor, defined as follows (see, e.g., Ref. [15]):

$$\boldsymbol{\sigma}_M = \mu_0^{-1}\left[\boldsymbol{B}\boldsymbol{B}^{\mathrm{T}} - \frac{1}{2}\|\boldsymbol{B}\|^2\mathbf{I}_3\right] \text{ on } \Gamma_N \tag{10}$$

where μ_0 denotes a magnetic permeability of vacuum, and $\mathbf{I}_3$ denotes a 3 by 3 identity matrix. The vector of magnetic force density is then represented as a traction vector of the Maxwell's stress tensor:

$$\boldsymbol{f}(\boldsymbol{x}, t) = \boldsymbol{\sigma}_M \cdot \boldsymbol{n}(\boldsymbol{x}) \text{ on } \Gamma_N. \tag{11}$$

Spatial discretization, such as the FEM, of the governing equations for the displacement field (Eqs. (1) through (3)), and those for the magnetostatic problem (Eqs. (7) through (9)) yields, the following semi-discrete governing equation:

$$\mathbf{M}\ddot{\mathbf{u}}(t) + \mathbf{C}\dot{\mathbf{u}}(t) + \mathbf{K}\mathbf{u}(t) = \mathbf{f}(t), \tag{12}$$

$$\mathbf{K}_M(\mathbf{A}) = \mathbf{j}(t), \tag{13}$$

where $\mathbf{M}$, $\mathbf{C}$, and $\mathbf{K}$ denote mass, damping, and stiffness matrices, $\mathbf{u}(t)$ is the discretized displacement vector, $\mathbf{f}(t)$ is the discretized magnetic force vector, $\mathbf{A}$ is a vector of the discretized magnetic vector potential, $\mathbf{j}$ is the magnetic load vector, and $\mathbf{K}_M$ is a vector of nonlinear functions with respect to $\mathbf{A}$. Here, we assume that the fluctuation in the displacement field does not alter the magnetic property of the electric machine. Therefore, we solve Eqs. (12) and (13) sequentially. Namely, we solve Eq. (13) for a given domain, and compute the magnetic force based on Eq. (10). The structural vibration problem is then solved using Eq. (12).

Given the magnetic force vector $\mathbf{f}(t)$, assuming that the magnetic force and the displacement field can be represented as harmonic functions in time, they are written as,

$$\mathbf{u}(t) = \mathrm{Re}\left(\mathbf{U}(\omega)\mathrm{e}^{\mathrm{j}\omega t}\right), \tag{14}$$

$$\mathbf{f}(t) = \mathrm{Re}\left(\mathbf{F}(\omega)\mathrm{e}^{\mathrm{j}\omega t}\right), \tag{15}$$

where $\mathrm{j} = \sqrt{-1}$, $\mathrm{Re}()$ denotes the real part, ω denotes angular frequency, $\mathbf{U}(\omega)$ and $\mathbf{F}(\omega)$ denote the frequency domain representation of $\mathbf{u}(t)$ and $\mathbf{f}(t)$, respectively. By substituting Eqs. (14) and (15) into Eq. (12), we obtain,

$$\boldsymbol{\mathcal{M}}(\omega)\boldsymbol{\alpha}(\omega) = \mathbf{F}(\omega), \tag{16}$$

where $\boldsymbol{\alpha}(\omega)$ denotes the vector of accelerations, or $\boldsymbol{\alpha}(\omega) = -\omega^2\mathbf{U}(\omega)$, $\boldsymbol{\mathcal{M}}(\omega)$ denotes the dynamic mass, or

$$\boldsymbol{\mathcal{M}}(\omega) = \mathbf{M} - \left(\frac{\mathrm{j}}{\omega}\right)\mathbf{C} - \left(\frac{1}{\omega^2}\right)\mathbf{K}. \tag{17}$$

Solving Eq. (16) with respect to $\boldsymbol{\alpha}(\omega)$ would yield,

$$\boldsymbol{\alpha}(\omega) = \boldsymbol{\mathcal{H}}(\omega)\mathbf{F}(\omega), \tag{18}$$

where $\boldsymbol{\mathcal{H}}(\omega) = \boldsymbol{\mathcal{M}}^{-1}(\omega)$ is a matrix of inertance, or herein referred to as a transfer function matrix.

Several attempts have been made to obtain accurate dynamic models of the electric machine stator assemblies based on FEAs [5–9]. However, they all require sophisticated modeling methods as well as model updating strategies. Most importantly, such models contain modeling errors. In this paper, we propose that $\boldsymbol{\mathcal{H}}(\omega)$ be replaced with experimentally obtained transfer function matrix, i.e.,

$$\boldsymbol{\alpha}(\omega) \simeq \tilde{\boldsymbol{\mathcal{H}}}(\omega)\mathbf{F}(\omega), \tag{19}$$

where $\tilde{\boldsymbol{\mathcal{H}}}(\omega)$ is the experimentally obtained transfer function matrix.

3. Analysis

This section provides the procedure of the proposed analysis framework, which consists of three steps:

(i) Computation of magnetic force vectors using given current waveforms

(ii) Measurement of transfer functions

(iii) Vibration synthesis based on Eq. (19)

These steps are described below.

3.1. Computation of magnetic force vectors

First, magnetostatic FEA needs to be conducted for solving the governing equations Eqs. (7) through (9). The resulting magnetic force vectors are then processed as follows. Figure 2 shows the schematics of the magnetic force vectors. The magnetic force is generated at the air-gap between the rotor and the stator core, which is a traveling-wave type excitation that moves along the circumferential direction at the air-gap. In this paper, we assume that the magnetic force is applied to each tooth as a resultant force, defined as follows:

$$\mathbf{f}_j(t) = \int_{\Gamma_j} f_r(\boldsymbol{x}, t)\mathbf{e}_r(\mathbf{x})\mathrm{d}\Gamma + \int_{\Gamma_j} f_\theta(\boldsymbol{x}, t)\mathbf{e}_\theta(\mathbf{x})\mathrm{d}\Gamma, \tag{20}$$

where $\mathbf{f}_j(t)$ is the resultant magnetic force acting on the jth tooth, $f_r(\boldsymbol{x}, t)$ and $f_\theta(\boldsymbol{x}, t)$ respectively denote the radial and the tangential components of the magnetic force vector, $\mathbf{e}_r(\boldsymbol{x})$ and $\mathbf{e}_\theta(\boldsymbol{x})$ denote the unit vectors along the radial and the tangential directions, respectively. $\mathbf{f}_j(t)$ should then be transformed to frequency domain representation $\mathbf{F}_j(\omega)$ by Fourier transform.

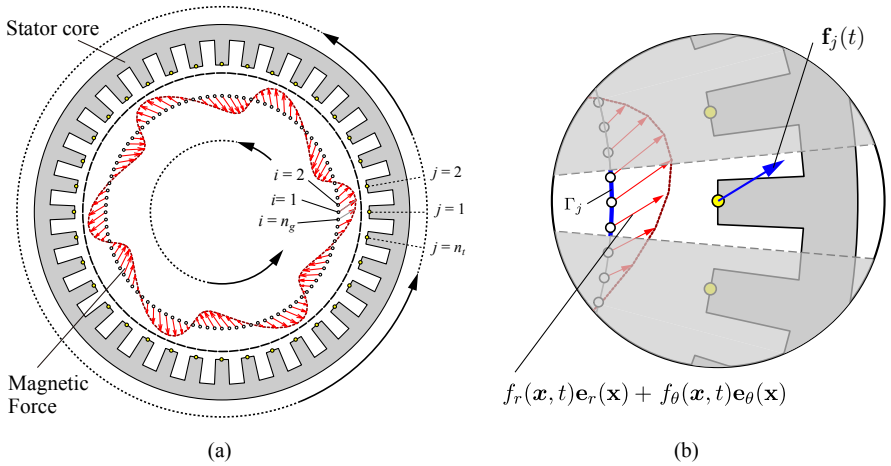

Figure 2. Schematics of magnetic force: (a) representative magnetic force distribution, (b) relationship between the distributed magnetic force and the its resultant force

3.2. Transfer function measurements

Second, transfer functions between the stator's teeth, and the response points of interests need to be measured by vibration testing using standard impact hammer or electrodynamic shaker, and FFT analyzers. Denoting inertance of the point of interest with respect to a point on the teeth as $\tilde{\mathcal{H}}_{rt}(\omega)$, it can be measured as,

$$\tilde{\mathcal{H}}_{rt}(\omega) = \frac{a_r(\omega)}{Q_t(\omega)} \tag{21}$$

where $a_r(\omega)$ denotes the acceleration at the point of interest, $Q_t(\omega)$ denotes the excitation force applied to the stator's teeth. It should be noted that the application of force to the teeth using electrodynamic shaker or impact hammer is not always feasible. Therefore, we apply force to the response points of interest, denoted here as $Q_r(\omega)$, and measure the resulting acceleration at the stator's teeth, $a_t(\omega)$. Reciprocity principle is then applied, i.e.,

$$\tilde{\mathcal{H}}_{rt}(\omega) = \tilde{\mathcal{H}}_{tr}(\omega) = \frac{a_t(\omega)}{Q_r(\omega)}. \tag{22}$$

The inertance should be measured between the response points of interest, and all the teeth. The measured inertances are then used to form the transfer function matrix $\tilde{\boldsymbol{\mathcal{H}}}(\omega)$ in Eq. (19).

3.3. Vibration synthesis

Using the frequency domain representation of the magnetic force vectors, and the measured transfer functions, vibration synthesis needs to be performed, based on Eq. (19). More specifically, it is written as follows:

$$\begin{bmatrix} \boldsymbol{\alpha}_1(\omega) \\ \vdots \\ \boldsymbol{\alpha}_m(\omega) \end{bmatrix} = \begin{pmatrix} \tilde{\boldsymbol{\mathcal{H}}}_{11}(\omega), & \dots, & \tilde{\boldsymbol{\mathcal{H}}}_{1n}(\omega) \\ \vdots & \ddots & \vdots \\ \tilde{\boldsymbol{\mathcal{H}}}_{m1}(\omega), & \dots, & \tilde{\boldsymbol{\mathcal{H}}}_{mn}(\omega) \end{pmatrix} \begin{bmatrix} \mathbf{F}_1(\omega) \\ \vdots \\ \mathbf{F}_n(\omega) \end{bmatrix}, \tag{23}$$

where m is the number of response points of interest, n is the number of teeth.

4. Experimental validation

In this section, the proposed analysis procedure is applied to an IPM machine, and the validity of the proposed analysis procedure is discussed. The photograph of the test bench used for the analysis is shown

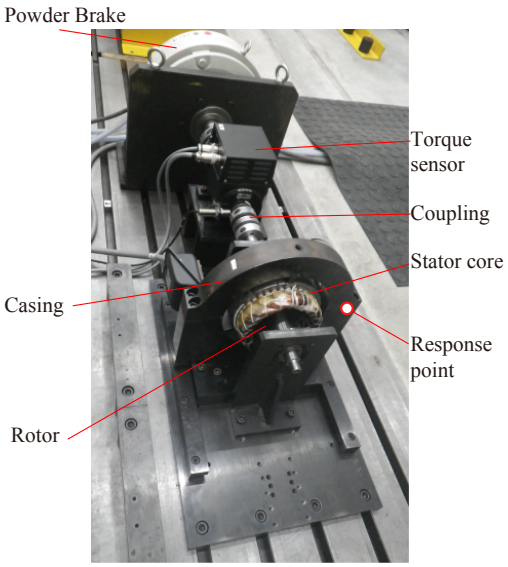

Figure 3. Test bench for the measurement of operational data

Table 1. Specification of the IPM machine

Rated power	2.2kW
Number of poles	6
Number of slots	36
Number of phases	3
Outer diameter of stator core	0.16m
Outer diameter of rotor core	0.099m

in Fig. 3, and the specificaiton of the electric machine used for the analysis is shown in Table. 1.

4.1. Analysis overview

The validation procedure is as follows. First, operational vibration (acceleration) data at a response point of interest was measured as reference data. The current data applied to the stator's windings for the three phases were also measured by current probes. During the operation of the motor, pulse-width modulation (PWM) control was used, which is a standard method for operating the brushless D.C. motors. The PWM control mimics a sinusoidal voltage by a train of rectangular pulse waves, which is achieved by repetitive turning on and off of the switch between the power supply and the electric load with very fast rate. The fundamental frequency of the resulting singal equals that of the sinusoid, but it contains higher harmonic contents. It is noted that from the standpoint of vibration and acoustic analyses, one of the most significant consequences of using the PWM control is that the resulting current and the magnetic field contain high-frequency components that stem from the integer multiples of the *carrier frequency* or the *switching frequency* in conjunction with their side-band spectra. Magnetic force induced by such magnetic field also contains high frequency components, which induces high frequency structural vibration and acoustic noise [3]. Second, by using the measured current data, magnetostatic calculations were conducted to obtain magnetic force vectors at the operational conditions. Third, vibration testing has been conducted to obtain the transfer function matrix. Finally, vibration synthesis has been performed by using Eq.(19).

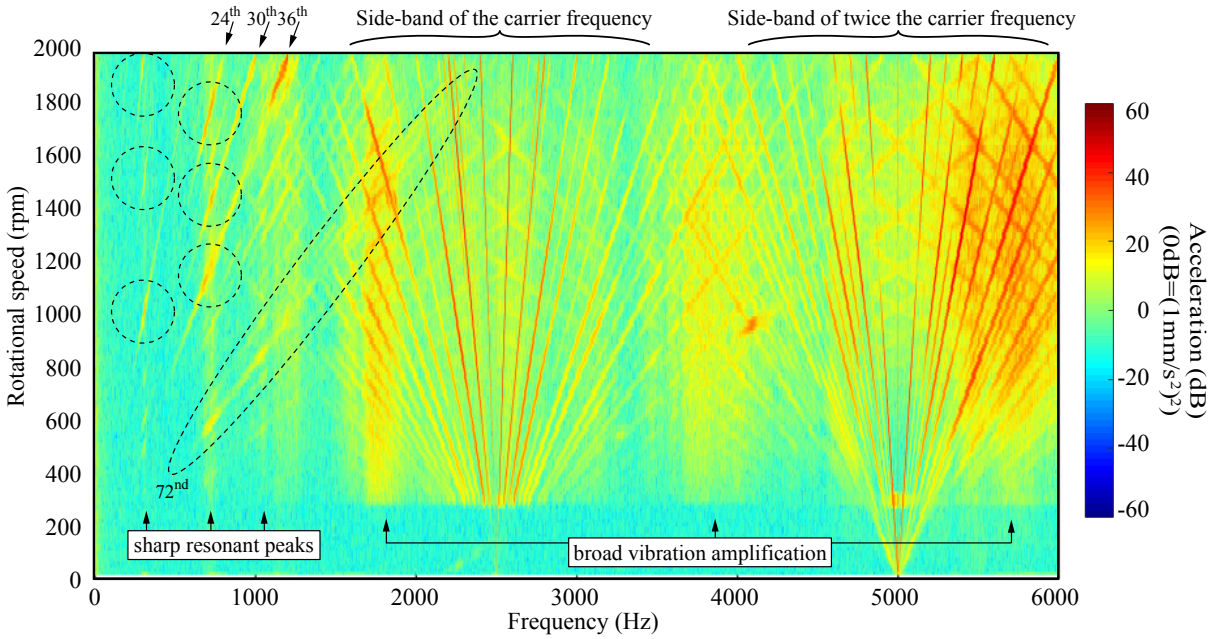

Figure 4. Frequency vs rotational speed for the measured acceleration

4.2. Measurement of operational data

The axial component of the acceleration at the response point of interest (Fig. 3) has been measured by using a triaxial accelerometer from 0 through 2,000rpm. The currents applied to the stator's windings were also measured so that the magnetic force during the operation can be computed. The carrier frequency for the PWM control was set to 2,500Hz. The frequency components of the measured acceleration were then computed by taking short time Fourier transform (STFT) of the measured time histories. The results are shown in Fig. 4 and discussed below.

There are two types of vibration peaks observed in the figure: (1) peaks that are dependent on the rotational speed, (2) the ones that are independent on the rotational speed. The former vibration peaks are shown as the order lines that originate from the origin, or the integer multiples of the carrier frequency (2,500Hz and 5,000Hz). The temporal orders of the lines originating from the origin are integer multiples of the number of poles (=6) of the rotor core. As can be seen, the lines of orders of 24, 30, and 36 appear in the plot. The line of order 72 is also significant. The latter peaks are related to the natural frequencies of the stator assembly. In Fig. 4, such peaks appear as vertical lines for sharp resonant peaks, or broad vibration amplification for the modes with large modal damping ratios. As can be seen in the figure, there are sharp resonant peaks at around 300Hz, 700Hz and 1,100Hz, for instance. On the other hand, the broad vibration amplification can be observed at around 1,900Hz, 4,000Hz, and 5,800Hz.

Furthermore, what complicates the vibration response of the electric motors is the combination effects between these vibration peaks. For instance, the 36th, 30th, and 24th order lines hit the resonant frequency of 700Hz at around 1,200rpm, 1,400rpm and 1,700rpm, respectively. Also, some of the order lines hit the resonant frequency of 300Hz at around 1,000rpm, 1,500rpm, and 1,900rpm, as indicated in the figure. These resonances are known to be caused by the interaction between the corresponding spatial components of the magnetic force and the vibration modes [16]. One of our goals in the proposed method is to accurately capture these vibration peaks by vibration synthesis.

4.3. Computation of magnetic force vectors

Using the measured current data, magnetostatic computations have been conducted by using the AC/DC module of the COMSOL Multiphysics®. It is noted that the magnetostatic computations have been

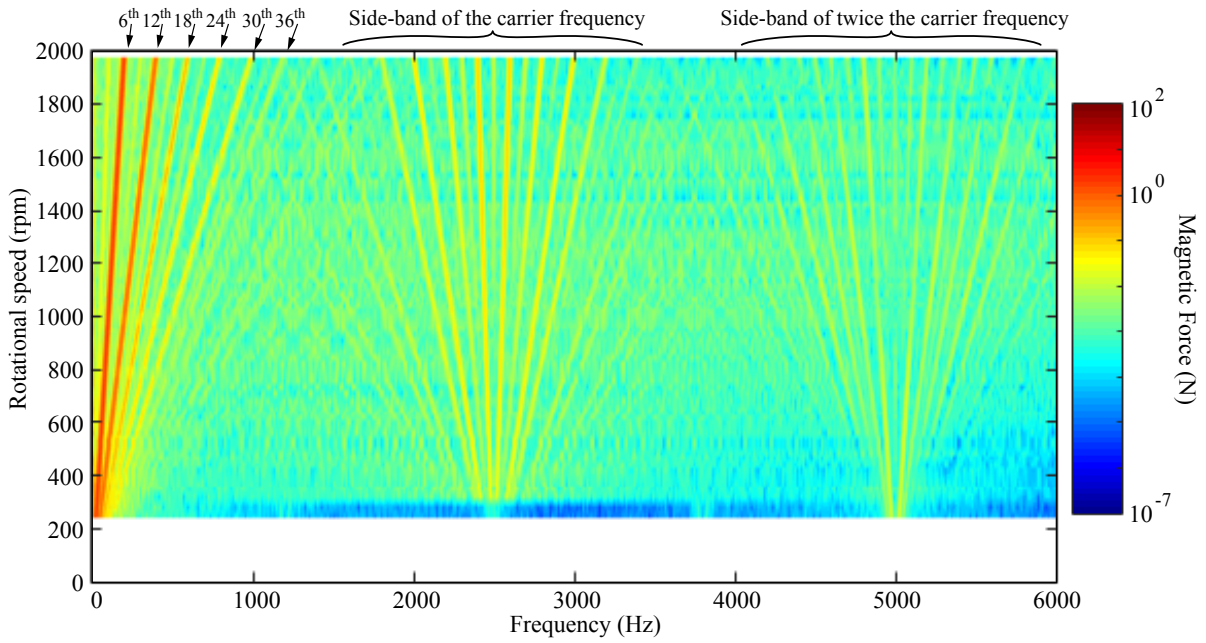

Figure 5. Frequency speed diagram of a radial component of the magnetic force applied to one of the teeth

conducted for one cycle of rotation, and sampling rate has been adjusted such that the resulting sampling frequency becomes 24,000Hz, which is fine enough to capture the spectrum in the frequency range of interest, even with the presence of PWM-caused side bands. The STFT was then applied to the computed magnetic force time histories and the representative result is shown in Fig. 5. The figure shows the STFT data of the magnetic force for one of the 36 teeth. As shown in Fig. 5, we can observe the lines with orders of the integer multiples of six. Side band peaks that originate from the carrier frequency, as well as twice the carrier frequency are also observed. Since many of these lines in Fig. 5 coincide with the ones found in Fig. 4, it implies that the ones in Fig. 4 are caused by the ones in the magnetic forces. However, the effect of these components on the vibration response is dependent on the modal characteristics of the stator assembly, as discussed next.

4.4. Transfer function measurement

The components in the transfer function matrix were measured by using the test setup shown in Fig. 6. As can be seen, the rotor was removed from the assembly, because its existence does not contribute to the modal characteristics of the stator assembly. Triaxial accelerometers were then placed on the surface of the stator's teeth, and the response point of interest was excited by an electromagnetic shaker in axial direction. A random burst excitation has been used. Averaging of the data for five measurements has been applied. The inertance was then computed by the FFT analyzer. The inertance measured at one of the teeth, as well as the coherence is shown in Fig. 7. There are sharp resonant peaks at around 300Hz, 700Hz and 1,100Hz, which were also observed in the operational data shown in Fig. 4. Furthermore, we can also see that the vibration levels at around 1,900Hz, 4,000Hz, and 5,800Hz are significant. The corresponding coherence values at these peaks are above 90%, as can be seen in Fig. 7(b). The coherence decreased for all three components below 300Hz. This appears to be because the vibration level becomes so small that the signal to noise ratio becomes small in this frequency range.

One thing to note here is that the radial and tangential components of the inertance are large at the sharp resonant peaks of 700Hz and 1,100Hz. For the electric motor used in this study, the dominant components of the magnetic force generated at the gap are the radial and the tangential ones. Therefore,

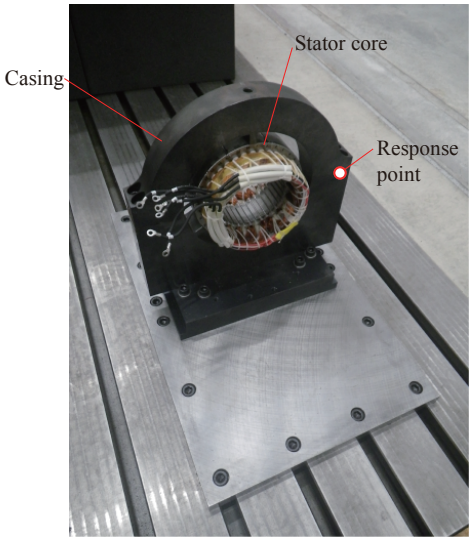

Figure 6. Test bench for the measurement of transfer function matrix

it partially explains the occurrence of the strong resonant peaks at 700Hz and 1,100Hz shown in Fig. 4, because these modes are highly sensitive to the radial and the tangential components of the external forces applied to the teeth.

4.5. Vibration synthesis

The magnetic force computed in 4.3, and the measured transfer functions described in 4.4 were used for the systhesis of the vibration response at the response location. The result of the synthesis is shown in Fig. 8. As can be seen in Fig. 8, the resonant peaks found in Fig. 4 are well captured by the proposed method. First, the synthesized vibration peaks that are dependent on the rotational speed match well with the measured ones. For instance, the lines of orders 24, 30 and 36 found in Fig. 4 are also seen in Fig. 8. The side-band spectra of the carrier frequency and those for twice that frequency also agree well with the measured ones. Moreover, the resonant peaks that are independent on the rotational speed also agree well with the measured counterparts. In particular, the combined effects of the natural frequencies and magnetic force are well captured by the method. In Fig. 8, the order lines of orders 12 and 18 hit the resonant peak of 300Hz at around 1,000rpm and 1,700rpm, respectively. Also at 700Hz, the order lines of order 24, 30, and 36 respectively show the resonance at around 1,200rpm, 1,400rpm and 1,700rpm, which agree well with those seen in Fig. 4.

Some discrepancies, however, are found between the synthesized and the measured results. First, in Fig. 8, the magnitude of the order lines of order 6, 12, and 18 is more significant than in Fig. 4 especially for the frequency range lower than 300Hz. This discrepancy appears to be attributed to the low coherence values in the frequency response below 300Hz, as shown in Fig. 7(b). Second, the resonant peaks related to the temporal order of 72 that appears in Fig. 4 cannot be seen in Fig. 8. This appears to be because the corresponding order of the magnetic force was not properly modeled by the magnetostatic FEA, since the line corresponding to the temporal order of 72 cannot be observed in Fig. 5 either. More accurate representation of the magnetic force vectors is necessary to accurately capture these vibration peaks.

It is noted that one of the most significant benefits of the proposed methodology is that the re-evaluation of the vibration response for different current profiles or rotor shapes does not require additional experiments during the development phase of the electric machines. When current profile and/or the rotor shape changes, one can synthesize the corresponding vibration response simply by re-calculating the

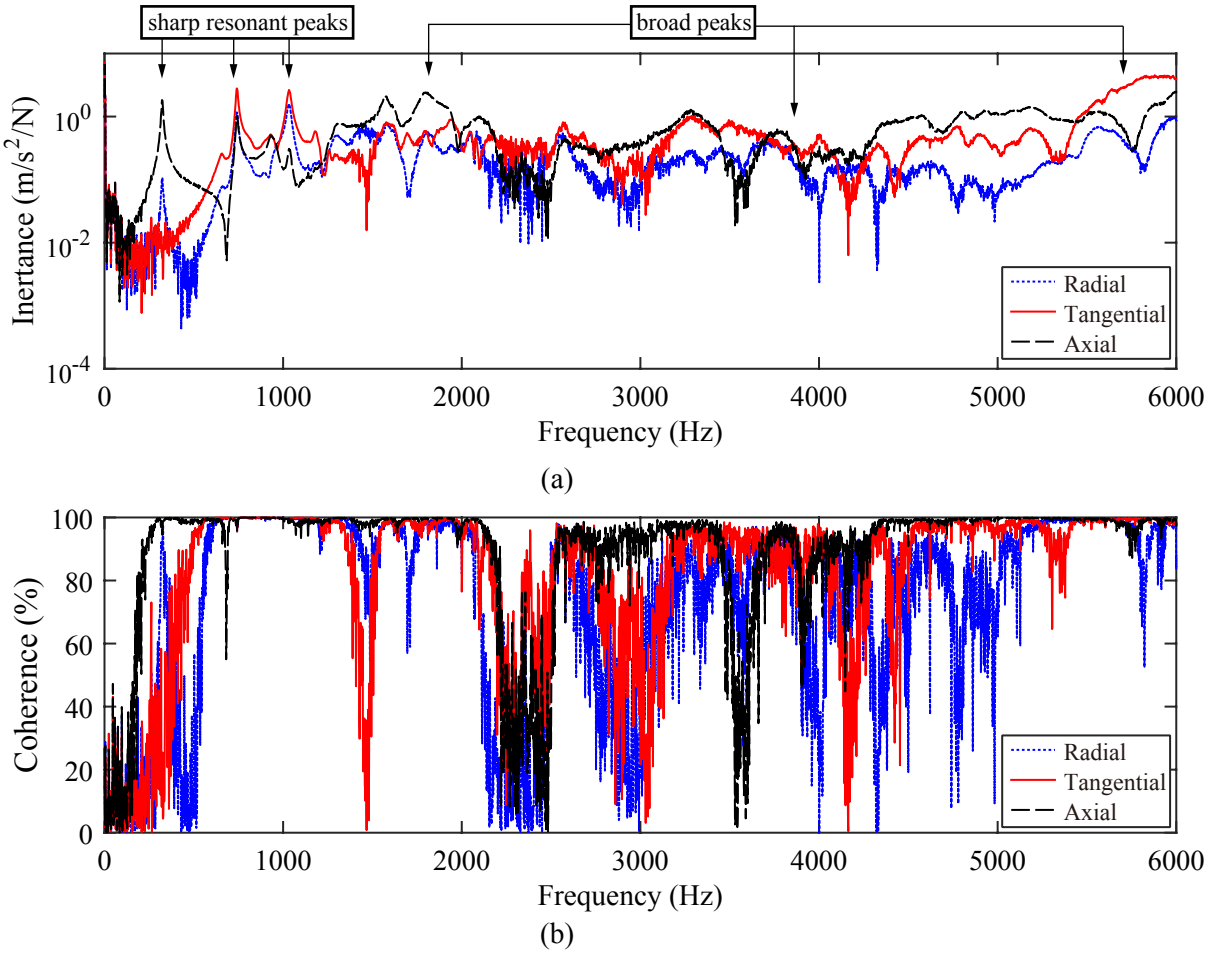

Figure 7. Frequency response of a typical point: (a) inertance, (b) coherence.

magnetic force vectors by magnetostatic FEA, which can be done quickly because it does not require additional experiments.

5. Conclusions and future work

In this paper, an accurate vibration prediction method for the electric machines has been proposed. The method utilizes experimentally-obtained structural transfer functions, and the magnetic forces computed by magnetostatic FEAs. The results show that the method is capable of predicting the vibration response of a specific point of interest of the stator assembly, for high frequency range, with high accuracy. Our future work will include the development of a more accurate representation of magnetic force and the coupling methodology, as well as more thorough investigations on the contributions from spatial components of both the vibration mode shapes and the magnetic forces.

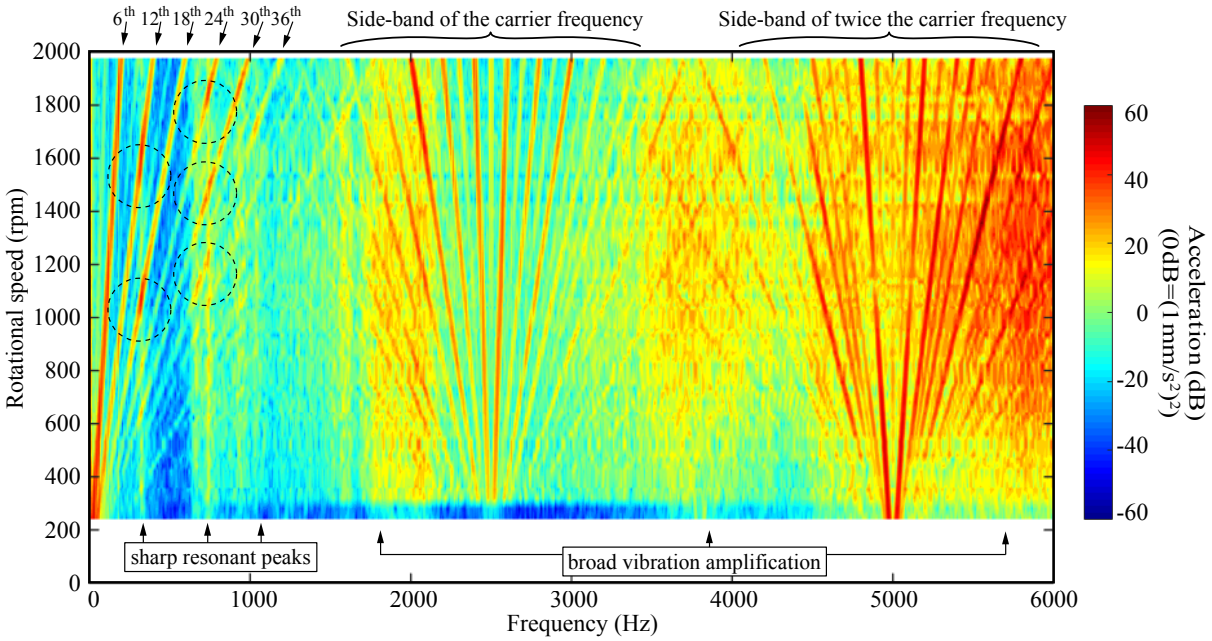

Figure 8. Frequency vs rotational speed for the synthesized acceleration

References

[1] K. Fonteyn, A. Belahcen, R. Kouhia, P. Rasilo, and A. Arkkio. FEM for directly coupled magneto-mechanical phenomena in electrical machines. *IEEE Transactions on Magnetics*, 46(8):2923—2926, 2010.

[2] M. Boesing, T. Schoenen, K.A. Kasper, and R.W. De Doncker. Vibration synthesis for electrical machines based on force response superposition. *IEEE Transactions on Magnetics*, 46(8):2986–2989, 2010.

[3] A. Saito, H. Suzuki, M. Kuroishi, and H. Nakai. Efficient forced vibration reanalysis method for rotating electric machines. *Journal of Sound and Vibration*, 334:388 – 403, 2015.

[4] J. Martinez, A. Belahcen, and J.G. Detoni. A 2D magnetic and 3D mechanical coupled finite element model for the study of the dynamic vibrations in the stator of induction motors. *Mechanical Systems and Signal Processing*, 66–67:640–656, 2016.

[5] G. Mogenier, T. N. Baranger, R. Dufour, L. Durantay, and N. Baras. Efficient model development for an assembled rotor of an induction motor using a condensed modal functional. *Journal of Computational and Nonlinear Dynamics*, 6(2):021011–021011, 10 2010.

[6] G. Mogenier, R. Dufour, G. Ferraris-Besso, L. Durantay, and N. Barras. Identification of lamination stack properties: application to high-speed induction motors. *IEEE Transactions on Industrial Electronics*, 57(1):281–287, 2010.

[7] M. van der Giet, K. Kasper, R. W. De Doncker, and K. Hameyer. Material parameters for the structural dynamic simulation of electrical machines. In *2012 XXth International Conference on Electrical Machines (ICEM)*, pages 2994–3000, Sept 2012.

[8] P. Millithaler, É. Sadoulet-Reboul, M. Ouisse, J.-B. Dupont, and N. Bouhaddi. Structural dynamics of electric machine stators: Modelling guidelines and identification of three-dimensional equivalent material properties for multi-layered orthotropic laminates. *Journal of Sound and Vibration*, 348:185 – 205, 2015.

[9] A. Saito, Y. Nishikawa, S. Yamasaki, K. Fujita, A. Kawamoto, M. Kuroishi, and H. Nakai. Equivalent orthotropic elastic moduli identification method for laminated electrical steel sheets. *Mechanical Systems and Signal Processing*, 72-73:607–628, 2016.

[10] R. Lin, A.N. Laiho, A. Haavisto, and A. Arkkio. End-winding vibrations caused by steady-state magnetic forces in an induction machine. *IEEE Transactions on Magnetics*, 46(7):2665 – 2674, 2010.

[11] B. Kaku, I. Miyashita, and S. Sone. A novel prediction method of acoustic magnetic noise based on induction motor's NHCC function. *IEEE Transactions on Industrial Electronics*, 46(2):398–406, 1999.

[12] K.-H. Ha, Y.-K. Kim, G.-H. Lee, and J.-P. Hong. Vibration reduction of switched reluctance motor by experimental transfer function and response surface methodology. *IEEE Transactions on Magnetics*, 40(2):577–580, 2004.

[13] D. Torregrossa, B. Fahimi, F. Peyraut, and A. Miraoui. Fast computation of electromagnetic vibrations in electrical machines via field reconstruction method and knowledge of mechanical impulse response. *IEEE Transactions on Industrial Electronics*, 59(2):839–847, 2012.

[14] C. Lin and B. Fahimi. Prediction of acoustic noise in switched reluctance motor drives. *IEEE Transactions on Energy Conversion*, 29(1):250–258, 2014.

[15] J. D. Jackson. *Classical Electrodynamics*. Wiley, 1998.

[16] Matthias Boesing. *Acoustic modeling of electrical drives — noise and vibration synthesis based on force response superposition*. PhD thesis, RWTH Aachen University, 2014.